Image Cover Sheet

CLASSIFICATION	SYSTEM NUMBER
UNCLASSIFIED	508975

TITLE

EXPERIMENTAL DATABASE DESCRIBING PULSE-TRIGGERED NONLINEAR INSTABILITY IN SOLID ROCKET MOTORS

System Number:

Patron Number:

Requester:

Notes:

DSIS Use only:

Deliver to:

Experimental Database Describing Pulse-Triggered Nonlinear Instability in Solid Rocket Motors

P. G. Harris and A. De Champlain

Reprinted from

Journal of Propulsion and Power

Volume 14, Number 4, Pages 429–439

AIAA

A publication of the
American Institute of Aeronautics and Astronautics, Inc.
1801 Alexander Bell Drive, Suite 500
Reston, VA 20191–4344

JOURNAL OF PROPULSION AND POWER
Vol. 14, No. 4, July–August 1998

Experimental Database Describing Pulse-Triggered Nonlinear Instability in Solid Rocket Motors

P. G. Harris*
Defence Research Establishment Valcartier, Val Bélair, Quebec G3J 1X5, Canada
and
A. De Champlain†
Laval University, Quebec, Quebec G1K 7P4, Canada

Pulse-triggered combustion instability constitutes a considerable problem in the design and operation of solid propellant rocket motors. Results from an experimental study involving 45 full-scale motor firings are presented to provide guidance in motor design and a database for comparison with existing and future nonlinear theories. The repeatability of pulse-triggered instability along with the effect of variations in propellant formulation, operating pressure, grain configuration, motor scale, and motor length were evaluated according to the parameters fraction of dc shift and wave strength. The stability rating of a configuration based on these two different parameters was not always consistent; the fraction of dc shift was judged superior. It was shown that oxidizer particle size distribution and the presence of a stability additive affected pulse-triggered instability. In addition, it was shown that instability tended to increase with pressure, that cylindrical grains tended to be less stable than star grains, that shorter motors tended to be less stable than longer ones, and that smaller motors tended to be less stable than larger ones.

Nomenclature

D	= diameter of a rocket motor
K_n	= ratio of burning surface area to nozzle throat area, restriction ratio
K_n^*	= value of K_n that defines the beginning of the unstable region, critical restriction ratio
L	= length of a rocket motor
p_{ac}	= shock-wave amplitude
p_{cs}	= time-averaged stable chamber pressure
p_{cs}^*	= time-averaged stable chamber pressure when $K_n = K_n^*$, critical pressure
p_{cus}	= time-averged unstable chamber pressure
p_{tr}	= minimum time-averaged stable chamber pressure at which a motor could be driven unstable at ignition, transition pressure
$(p_{ac} + p_{cus})/p_{cus}$	= wave strength
$(p_{cus} - p_{cs})/p_{cs}$	= severity of instability for $p_{cs} = 8.3$ MPa, degree of instability or fraction of dc shift when p_{cs} assumes any value
ϕ	= mass-fraction of propellant burned

Introduction

DURING the operation of solid rocket motors, the passage of ejecta through the nozzle will create a small compression wave that can grow into a large-amplitude steep-fronted wave (shock wave). This wave is usually accompanied by an increase in the time-averaged operating pressure of the motor (Fig. 1). This type of instability is often referred to as pulse-triggered nonlinear longitudinal combustion instability (identified from here on as pulse-triggered instability). The shock wave and the increased time-averaged operating pressure can have serious consequences on motor performance, ranging from a changed thrust-time profile, to damaged missile electronics, to catastrophic failure of the motor. Because of the high cost of pulse-triggered instability in terms of system performance and dollars required to correct problems occurring in motors under development or those already in service, considerable effort has been invested in its understanding and the development of design methods to avoid or minimize its occurrence.

Experimental study of pulse-triggered instability at the Defence Research Establishment Valcartier (DREV) began in the early 1960s. The foundational work carried out by Bownlee and Roberts[1,2] and later built upon by Smith et al.[3] and Hughes and Smith[4] produced an extensive database of hundreds of pulsed-motor firings characterizing the effect of propellant formulation, propellant burning rate, initial propellant temperature, motor scale, and grain configuration. Early propellant formulations were based on polyurethane (PU) and ammonium perchlorate (AP). However, work expanded with time to include carboxyl-terminated polybutadiene (CTPB) and hydroxyl-terminated polybutadiene (HTPB) binders. Other formulation variants included the effect of aluminum, burning rate modifiers, oxidizer particle size distribution, and binder level. Motors fired varied in size from 51 mm in diameter and 254 mm long to 432 mm in diameter and 4570 mm long. Grain configurations included full-length cylinders, stars, arms, split-cylinders, and slotted tubulars. A single grain having a cylindrical and a slotted tubular cross section was also tested.

Despite the extensive work already done,[1–4] an additional test program involving pulsed-motor firings was considered worthwhile. There were three main reasons for this decision. Firstly, although the previous work includes some results for the more modern HTPB propellant systems, the major quantity were for PU and CTPB systems. Secondly, any present attempt at high-frequency analysis of the data would be seriously limited by the form and/or quality of the data: many of the high-frequency data records were on 35-mm strip film and the quality of the data was affected either by large gas cavities between the transducer diaphragm and the combustion chamber, centerline mounting of the pressure transducer, or by a highly viscous zinc-oxide putty used as a protective coating for the transducer. Finally, the lack of pressure-coupled combustion response measurements make a comparison of the experi-

Received Dec. 4, 1997; revision received April 4, 1998, accepted for publication April 6, 1998.

*Leader, Propulsion Group, Delivery Systems Section. Member AIAA.
†Professor, Mechanical Engineering. Member AIAA.

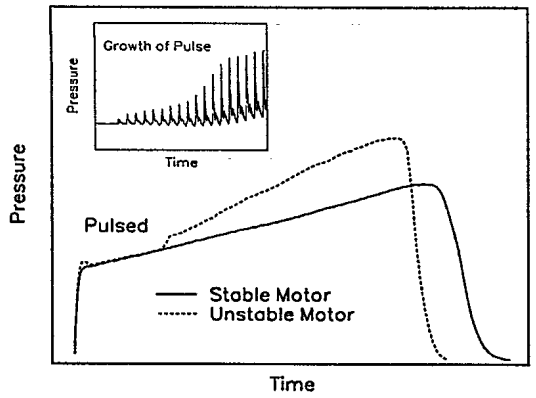

Fig. 1 Example of pulse-triggered combustion instability.

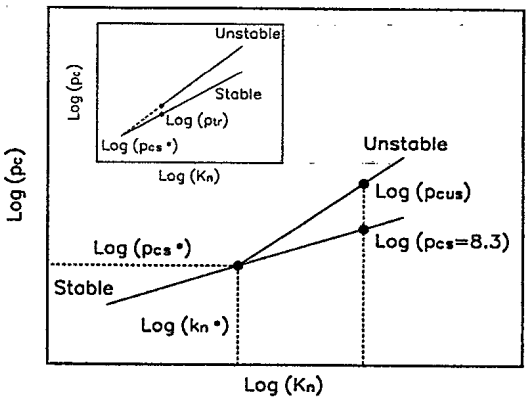

Fig. 2 Log–log relationships between p_c and K_n.

mental results with existing analytical and numerical models impossible. The present study was designed to take these reasons into account.

The experimental results presented in this paper are from the Canadian contribution to a joint international study of pulse-triggered instability. Some of the U.S. results have already been reported by Blomshield et al.[5] The combined results from this joint study and a previous study by Aerojet Solid Propulsion Company and Phillips Laboratory[6] form an extensive database that will assist motor designers and facilitate the evaluation of existing and future theoretical models. The emphasis of this paper is the presentation of a time-domain analysis of the experimental results of the Canadian contribution. Frequency-domain analyses and comparison with the Baum et al.[6,7] numerical code are planned for a future publication.

The experimental data in this paper are presented using two parameters: Fraction of dc shift and wave strength. These parameters are based on previous work at DREV and as such we begin our discussion with an explanation of their origin and definition. This discussion is followed by a presentation of the experimental test matrix and methodology, and then by a short section on instrumentation and data acquisition. Next, the complete set of time-averaged pressure traces is presented providing background information to facilitate a more complete understanding of the analysis based on the fraction of dc shift at the end of the paper. A discussion of the repeatability of pulse-triggered instability for motors from the same propellant batch and for motors from different batches is then pursued based on the time-averaged pressure traces. The remainder of the paper focuses on an analysis of the effect of different motor parameters on pulse-triggered instability as characterized by the fraction of dc shift and wave strength.

Stability Criteria

The evaluation in this paper of the influence of different motor configurations on pulse-triggered instability was done on the basis of two parameters: Fraction of dc shift and wave strength. In this section we explain their origin and definition.

Early in the work at DREV a strong log–log correlation was recognized to exist between p_{cus} and K_n. This is illustrated in Fig. 2. For many propellants the slope of the unstable portion of the curve was greater than that of the stable portion such that the two curves intersected. The pressure and restriction ratio at this point of intersection were identified as p_{cs}^* and K_n^*, respectively. It was concluded that below these values a given motor would be intrinsically stable and, thus, they became a measure of the stability of a propellant in a given motor. Although further testing indicated that the values of p_{cs}^* and K_n^* were dependent on motor size and to a certain extent on motor length (for $L/D < 10$ irregular behavior was observed), these parameters were considered valid for rating a propellant in a given motor configuration.

When work began on CTPB/AP propellant systems, the similarity in the slopes of the stable and unstable portions of the curves resulted in the value of p_{cs}^* being unrealistically low such that propellants could only be pulsed unstable at pressures significantly greater than p_{cs}^*. This is illustrated in the inset to Fig. 2. Consequently, another pressure parameter, p_{tr}, was defined as the minimum operating pressure at which a motor could be driven unstable at ignition. The definition of p_{tr} at ignition was to account for the effect of web fraction burned.

The primary emphasis of previous work was the definition of limits of intrinsic instability, thus the choice of parameters such as p_{cs}^* and p_{tr}. However, two other parameters were also used to characterize a motor once operating unstably. The first, severity of instability, quantified the fractional increase in the time-averaged operating pressure $(p_{cus} - p_{cs})/p_{cs}$. This was defined for a specific value of p_{cs}, such as 8.3 MPa (Fig. 2). The second parameter, wave strength, quantified the strength of the shock wave and was defined as the ratio of the sum of p_{ac} plus the time-averaged unstable pressure to the time-averaged unstable pressure $(p_{ac} + p_{cus})/p_{cus}$.

Given the emphasis of the present experimental work on characterizing instability once present, the two parameters, severity of instability and wave strength, formed the basis of the time-domain analysis. The severity of instability was adapted to be applied throughout a given firing and not restricted to a p_{cs} of 8.3 MPa. This adapted parameter, which was called the fraction of dc shift, characterized the effect of instability on the change in time-averaged pressure. The wave strength was used to characterize the propagating wave throughout the firing. Although the web fraction that was burnt is recognized to be of importance, it was not accounted for in the present analysis nor was it considered to be significant enough to change final conclusions.

Test Matrix and Methodology

The test matrix was comprised of 45 full-scale motor firings divided into 11 test cases and included variations in propellant formulation, operating pressure, grain configuration, motor length, and motor scale; repeatability was also investigated.

The test cases are described in Table 1. Three nonaluminized HTPB/AP propellant formulations were considered. Their compositions are given in Table 2 and representative results for the mean particle size of each lot of granular ingredients are given in Table 3. The Fisher Subsieve and Alpine Air-Jet Sieve methods provide a mean particle size measurement, whereas, the Coulter Counter values are based on a distribution. Coulter Counter measurements of Fe_2O_3 and $ZrSiO_4$ were performed with an aperture size of 50 μm, thus limiting the smallest measurable particle size to 1 μm. The Coulter Counter measurements of AP were made using an aperture of 280 μm. Unfortunately, the accuracy of these results is questionable given the problem of the solubility of AP in the electrolyte.

Table 1 Experimental test matrix

Test case	Diameter, mm	Length, mm	Grain geometry	Propellant formulation	Reference pressure, MPa	Reference, K_n
1	64.8	777	Cylinder	A	12.4	307.8
2	64.8	777	Cylinder	B	12.4	307.8
3	64.8	777	Cylinder	C	12.4	307.8
4	64.8	518	Cylinder	A	12.4	307.8
5	64.8	518	Star A	A	12.4	307.8
6	64.8	518	Star A	A	13.8	331.4
7	64.8	518	Star A	A	15.2	354.3
8	64.8	777	Stepped-cylinder	A	12.4	307.8
9	64.8	777	Star B	A	12.4	307.8
10	119.8	1438	Cylinder	A	12.4	307.8
11	119.8	1438	Star B	A	12.4	307.8

Table 2 HTPB/AP propellant formulations

Ingredient	Propellant A, wt %	Propellant B, wt %	Propellant C, wt %
AP			
400/200/17 μm in parts of 2/3/5	58.30	58.07	——
400 μm	11.66	11.61	27.1
200 μm	17.49	17.42	27.1
50 μm	——	——	10.1
20 μm	——	——	23.1
$ZrSiO_4$	——	0.5	——
Fe_2O_3	0.55	0.4	0.6
Binder	12.0	12.0	12.0

Table 3 Ingredient mean particle sizes

		Mean particle size		
Ingredients	Lot number	Fisher subsieve	Alpine air-jet sieve	Coulter counter
Fe_2O_4	TP-7913	0.500	——	1.5
$ZrSiO_4$	TP-82125	0.625	——	1.55
AP 400 μm	TP-8454	——	410	——
AP 200 μm	TP-8455	——	195	——
AP 400/200/17 μm	TP-8456	——	105	——
AP 50 μm	G-135	11.7	——	52
	G-139	12.1	——	51
AP 20 μm	G-144	5.9	——	22.2
	G-147	5.5	——	22.0

Previous studies at DREV concentrated on the effect of significantly different propellant burning rates on pulse-triggered instability.[2–4]. However, in the present study the steady burning rate at 6.9 MPa was maintained constant at 12.27 mm/s with maximum variations of −2.3 and +2.7%. The pressure exponent varied between 0.342 and 0.390. The purpose was to determine what change in pulse-triggered instability could be evoked by a motor designer when the stable burning rate was a fixed design parameter.

Pressure-coupled response function measurements of the three propellant formulations were carried out by the U.S. Naval Air Warfare Center using a T-burner. All propellants were evaluated at 12.4 MPa. In addition, propellant A was also evaluated at 6.9 and 15.2 MPa, to account for the variation in reference pressure associated with test cases 5–7. Limitations in the T-burner design required that the testing be carried out at pressures that were lower than maximum values encountered in the full-scale motor firings. The results of the response function measurements are given in Figs. 3 and 4. Figure 3 shows the pressure-coupled response increasing with pressure for propellant A up to 12.4 MPa followed by a decrease at 15.2 MPa. In Fig. 4, propellant A has the highest peak response, followed by propellants C and B.

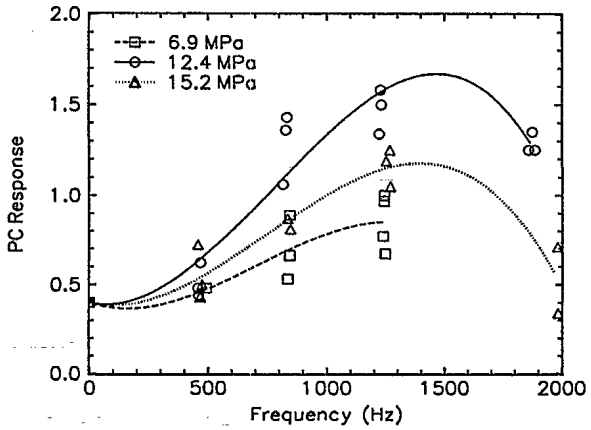

Fig. 3 Pressure-coupled combustion response for propellant A.

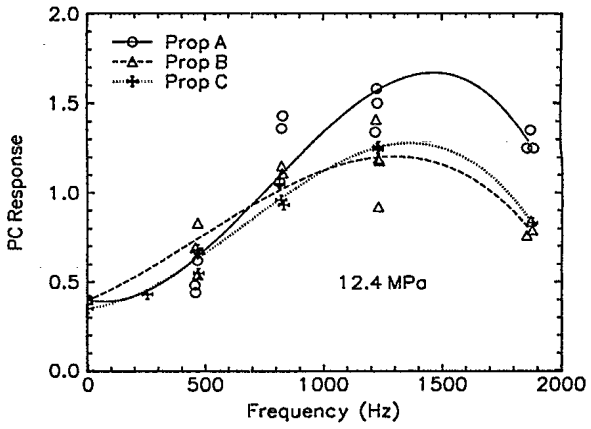

Fig. 4 Pressure-coupled combustion response for propellants A, B, and C.

The different grain configurations along with the motor scale and length variations are shown in Fig. 5. The designation 03020-C identifies a cylindrical grain with a nominal diameter of 3 in. and a nominal length of 20 in.; the experiment was designed using the British system of units. The grain configurations SA and SB are for two different star variations, A and B, and StC identify a stepped-cylinder configuration.

For each test case, at least one unpulsed motor firing was carried out. This firing was compared with the results of the ballistic module of the standard performance prediction code (SPP)[8] where ballistic parameters, including the stable burning rate, were varied to give optimum agreement between the experimental and theoretical pressure curves. The results of this calculation for test case 2 are illustrated in Fig. 6, the unpulsed case. The parameters from SPP were then used to generate

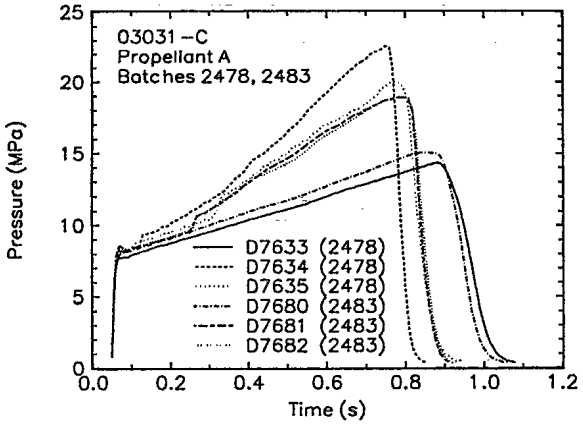

Fig. 8 Time-averaged pressure traces for test case 1.

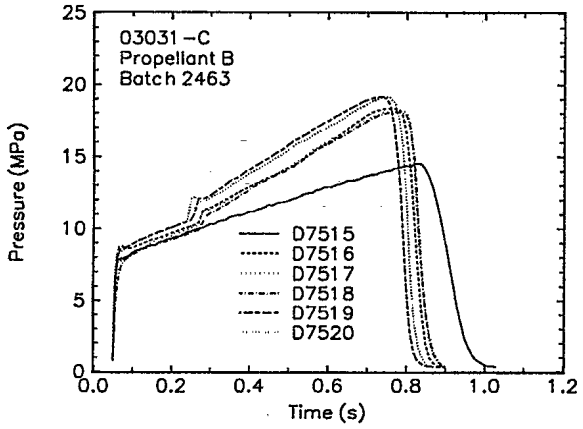

Fig. 9 Time-averaged pressure traces for test case 2.

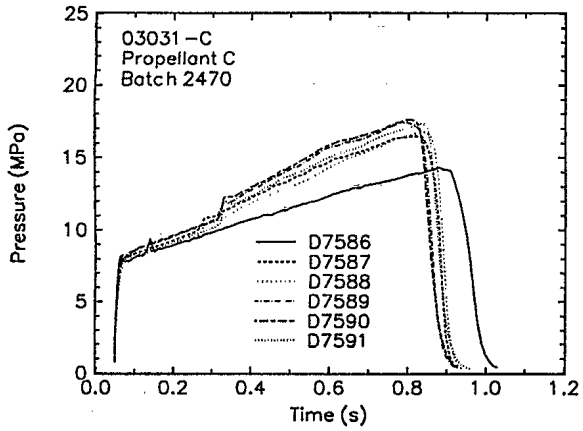

Fig. 10 Time-averaged pressure traces for test case 3.

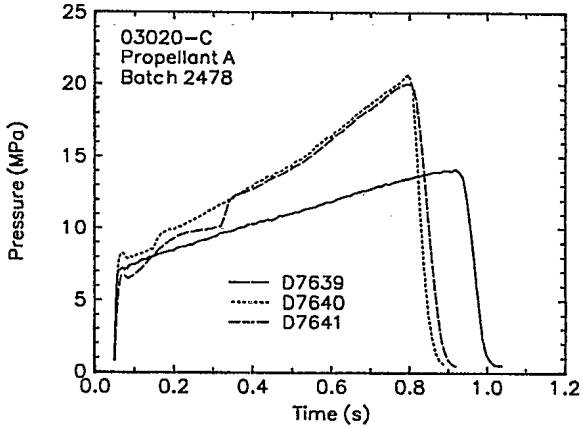

Fig. 11 Time-averaged pressure traces for test case 4.

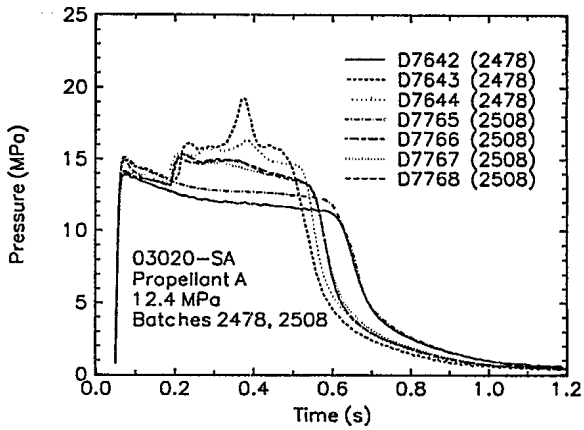

Fig. 12 Time-averaged pressure traces for test case 5.

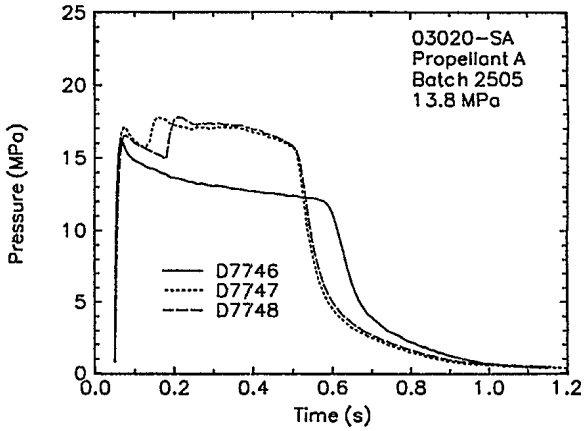

Fig. 13 Time-averaged pressure traces for test case 6.

the time-averaged pressures compared. No comparison was made between the two test cases because they were for different propellants and, therefore, different batches.

To get a quantitative idea of the repeatability of the time-averaged pressure, its variation around the mean value at $\phi = 0.5$ was calculated for each test case; ϕ was chosen instead of time because equal values of ϕ gave similar internal grain geometries. The variation on the mean for test cases 2 and 3 was ± 4.3 and 4.5%, respectively. However, close examination of the data showed that a significant portion of the variation was probably not because of pulse-triggered instability. Rather it was because of differences in three quantities: Time-averaged pressure traces before pulsing, pulsing times and to a lesser extent, initial pulse amplitudes. Therefore, for motor firings that did not have these differences, repeatability of the pulse-triggered phenomenon was considerably better.

Repeatability Between Batches

The effect of batch-to-batch propellant variation on pulse-triggered instability was investigated with test cases 1 and 5. The question being asked was whether normal variations in propellant formulation associated with different batches significantly effected pulse-triggered instability. Each test case was principally examined on its own, given the difference in grain configuration and propellant batches.

Test case 1 (Fig. 8) indicated little effect of propellant batch and, therefore, reasonable repeatability for the 03031-C configuration.

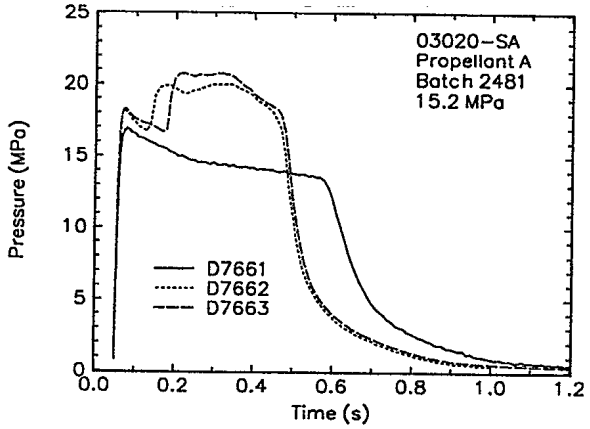

Fig. 14 Time-averaged pressure traces for test case 7.

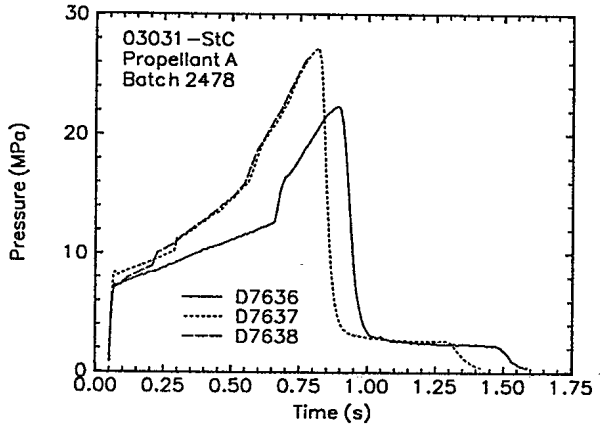

Fig. 15 Time-averaged pressure traces for test case 8.

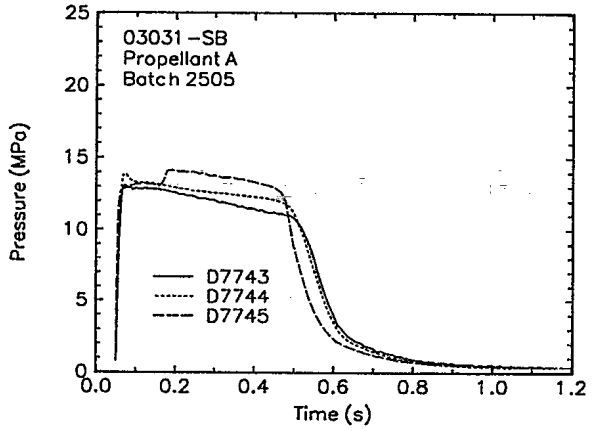

Fig. 16 Time-averaged pressure traces for test case 9.

Significant differences in the time-averaged pressure traces were seen for the two batches of test case 5 (Fig. 12). This was in spite of the fact that propellant ingredients for the two batches came from the same lots and that stable burning rates were similar. It was noted that batch 2478 did not give the same anomalous behavior for the 03031-C configuration as it did for the 03020-SA one. Therefore, it was concluded that there was a probable influence of the grain configuration. In particular, the 03020-SA configuration operated in the region of a stability boundary. It is believed that the boundary was related to a critical interaction between pulse-triggered instability and transverse pressure oscillations.

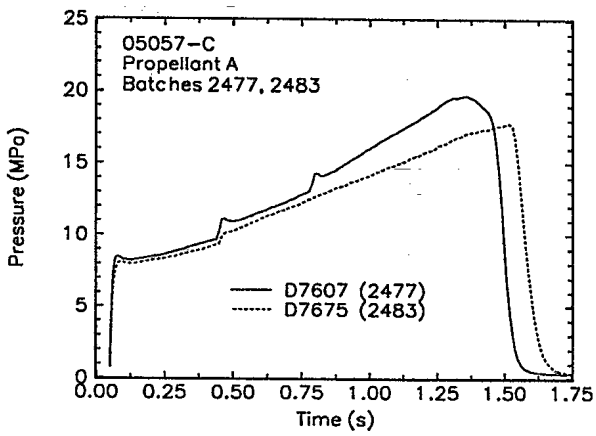

Fig. 17 Time-averaged pressure traces for test case 10.

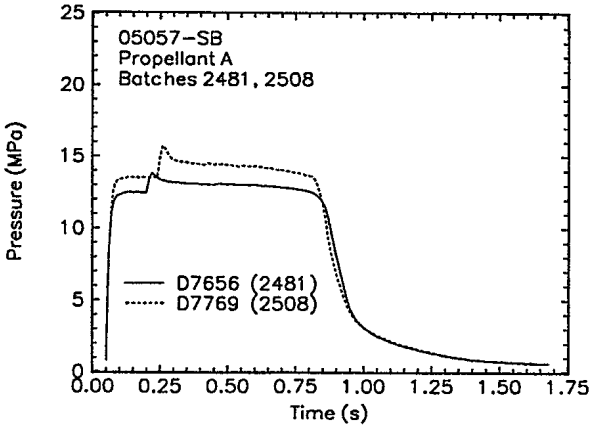

Fig. 18 Time-averaged pressure traces for test case 11.

Pulsed Motor Behavior

The effect of different motor parameters on pulse-triggered instability and its repeatability are of prime interest to a motor designer. The question of repeatability was first addressed in the previous section from the perspective of time-averaged pressure. In this section it is addressed from the perspective of the fraction of dc shift and wave strength. In addition, the effect of propellant formulation, operating pressure, grain configuration, motor size and length, and double shock-wave system are also evaluated.

The data for the present analysis are presented in Figs. 19–32. The fraction of dc shift is plotted as a function of p_{cs} and the wave strength is plotted as a function of p_{cus}. These were chosen because of their direct physical relationship to the parameters representing the instability, the fraction of dc shift being defined as $(p_{cus} - p_{cs})/p_{cs}$ and wave strength being defined as $(p_{ac} + p_{cus})/p_{cus}$.

Repeatability

The repeatability of pulse-triggered instability based on the fraction of dc shift and the wave strength is examined in Figs. 19 and 20, respectively. The graphs are for the 03031-C configuration and the three propellant formulations.

As with the discussion of repeatability based on the time-averaged pressure, the extent to which the fraction of dc shift and wave strength were similar for different motors from a given test case was considered as a measure of the repeatability of pulse-triggered instability.

In Fig. 19, the fraction of dc shift for propellant B (test case 2) showed the least repeatability, within approximately ±25% of the average and for propellant A (test case 1) showed the greatest repeatability, within approximately ±10%. The vari-

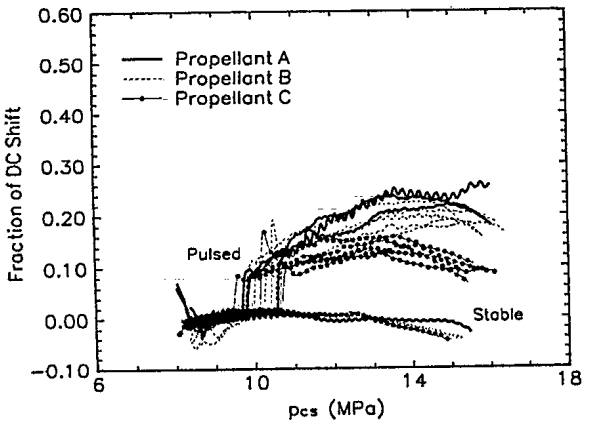

Fig. 19 Repeatability of the fraction of dc shift and the effect of propellant formulation.

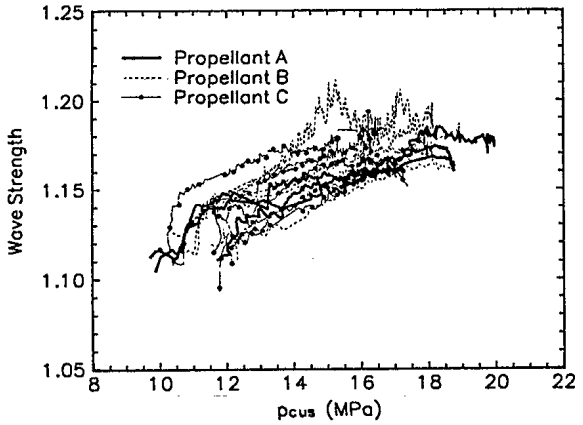

Fig. 20 Repeatability of the wave strength and the effect of propellant formulation.

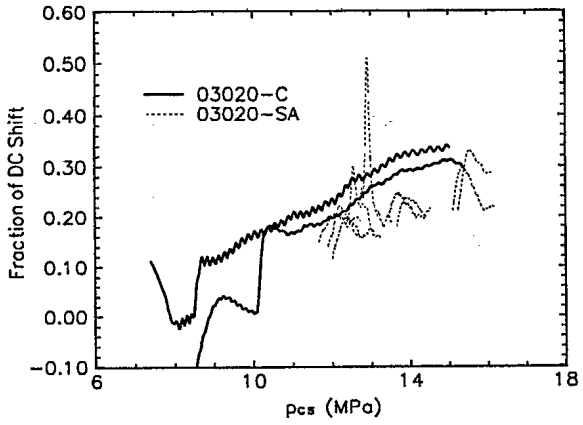

Fig. 21 Effect of operating pressure and grain configuration on the fraction of dc shift.

ability of the fraction of dc shift was greater than that of the time-averaged pressure because percent variation in the first case was calculated on a small number rather than a large one as in the latter case. However, as with the time-averaged pressure, the lack of repeatability was more a result of the test method than of pulse-triggered instability.

The wave strength (Fig. 20) was more repeatable than the fraction of dc shift, with propellant B being the least repeatable, within approximately ±1.7% of average values and propellant A being the most repeatable, within ±0.6%. Even when a more sensitive parameter was used, the ratio of the shock-

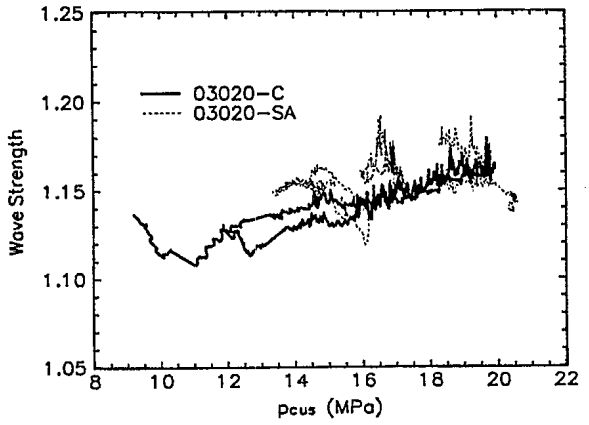

Fig. 22 Effect of operating pressure and grain configuration on the wave strength.

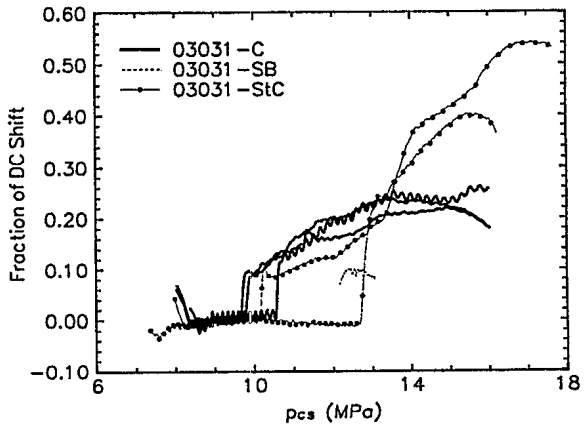

Fig. 23 Effect of grain configuration on the fraction of dc shift.

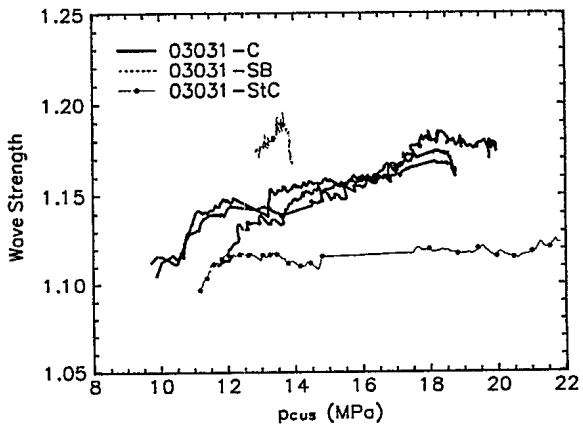

Fig. 24 Effect of grain configuration on the wave strength.

wave amplitude to the unstable time-averaged pressure p_{ac}/p_{cus}, the maximum variability did not exceed ±12.3%.

Effect of Propellant Formulation

The effect of propellant formulation on pulse-triggered instability based on the fraction of dc shift and the wave strength is also examined in Figs. 19 and 20, respectively.

Based on the fraction of dc shift (Fig. 19), propellant A tended to be the least stable propellant, followed by B and C, the difference becoming more pronounced as a firing proceeded. In addition, the profile of the fraction of dc shift seemed to vary between propellants. The most remarkable dif-

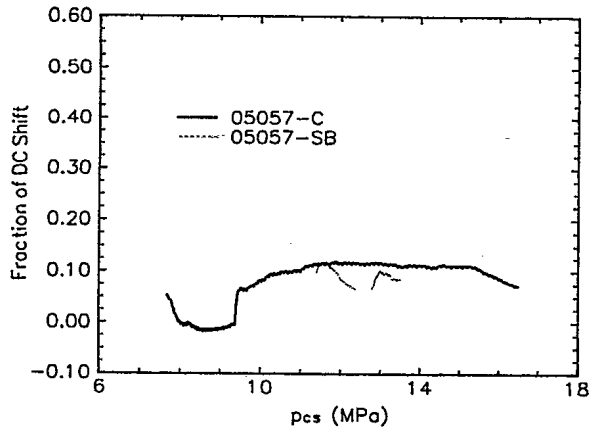

Fig. 25 Effect of grain configuration on the fraction of dc shift.

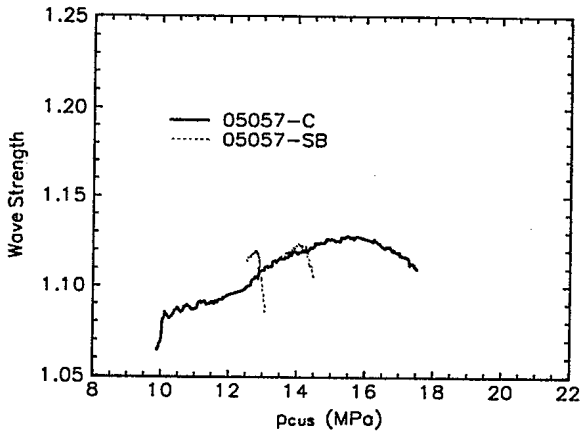

Fig. 26 Effect of grain configuration on the wave strength.

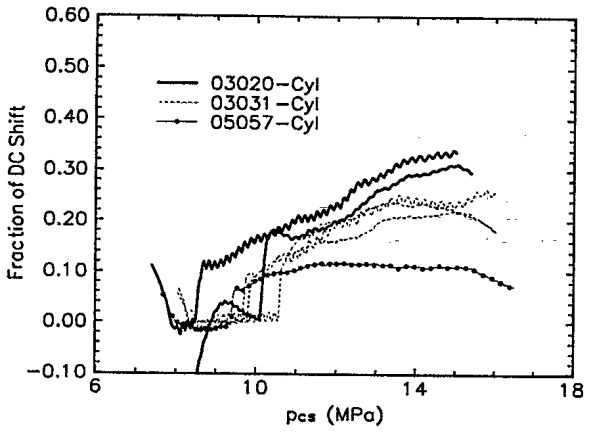

Fig. 27 Effect of motor size and length on the fraction of dc shift.

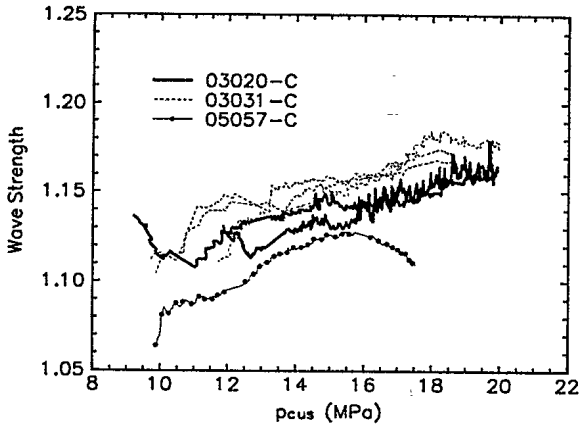

Fig. 28 Effect of motor size and length on wave strength.

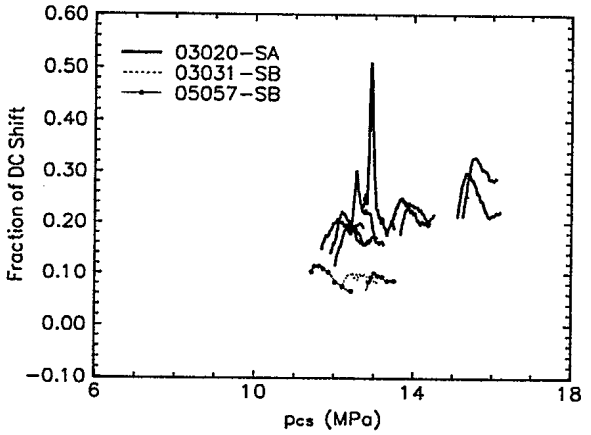

Fig. 29 Effect of motor size and length on the fraction of dc shift.

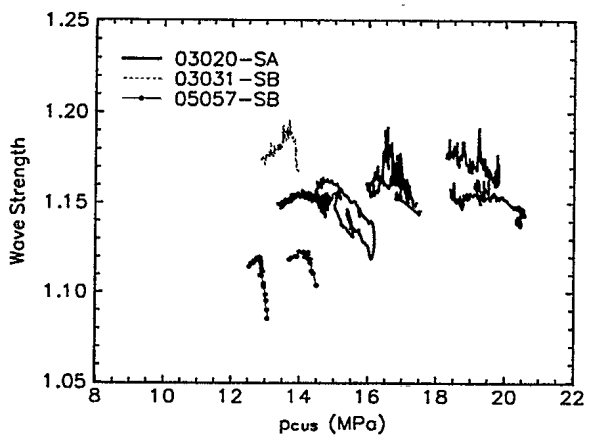

Fig. 30 Effect of motor size and length on the wave strength.

ference was the negative slope for propellant C after approximately 13.25 MPa.

Unlike the fraction of dc shift, no easily identifiable difference existed for the average values of the wave strength for the different propellants (Fig. 20); the propellants tended to have similar stability. Two of the six firings from propellant B were an exception to this in that they showed considerable excursions in the wave strength around 15 and 17 MPa. The general difficulty in establishing a difference in the stability of the propellants based on the parameter of wave strength compared to the discernable difference in stability based on fraction of dc shift indicated a decoupling of the two parameters.

When the stability ranking based on the fraction of dc shift (Fig. 19) was compared with the propellant formulations (Table 2) two conclusions were drawn. Firstly, particle size distribution of the AP affected the fraction of dc shift. Whether this effect resulted from the presence of more large particles (propellant A) or a greater spread in the distribution (propellant C), is impossible to say. Secondly, the addition of the stability additive in propellant B, $ZrSiO_4$, made the propellant more stable.

It is interesting to note that the propellant that was the least stable according to the fraction of dc shift, A, had a peak linear pressure coupled response that was greatest (Fig. 4). The similarity breaks down, however, for propellants B and C, where according to the peak value of the linear pressure-coupled response, propellant C should have been marginally less stable

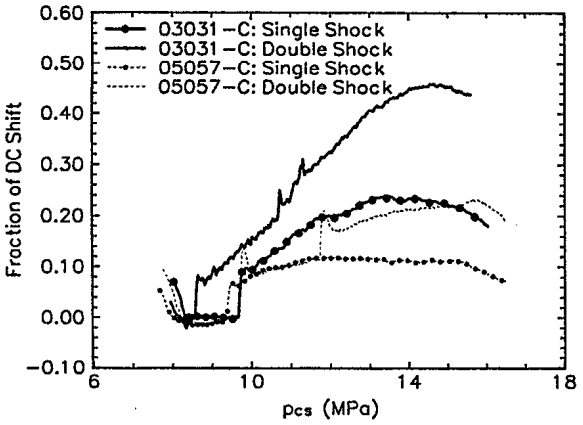

Fig. 31 Effect of double-shock systems on the fraction of dc shift.

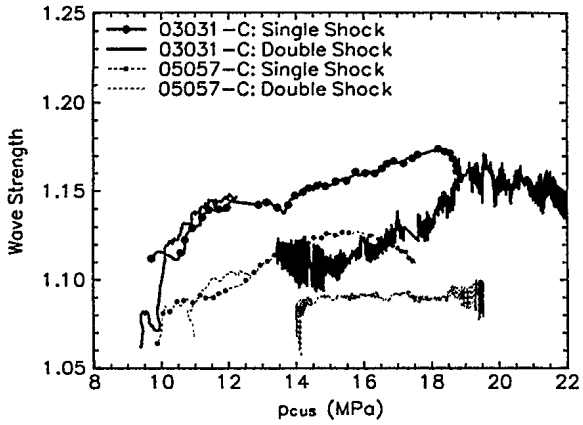

Fig. 32 Effect of double-shock systems on the wave strength.

than B. This difference is not surprising because this type of reasoning does not account for the multimodal nor the nonlinear nature of pulse-triggered instability.

Effect of Operating Pressure and Grain Configuration (03020-C/-SA)

The effect of operating pressure and grain configuration on pulse-triggered instability based on the fraction of dc shift and the wave strength are illustrated in Figs. 21 and 22, respectively. The graphs are for the 03020-C and 03020-SA configurations.

Figure 21 indicates that the fraction of dc shift and, thus, instability, increased with pressure for both the cylinder and the star, being greater for the cylinder. The large peak for the star configuration at 13 MPa was for motor D7643, and resulted from a tangential mode oscillation. The variation in the fraction of dc shift for the majority of the star motors was large for the change in magnitude of p_{cs}. It is believed that a considerable amount of this variation was also the result of transverse mode oscillations and that the fraction of dc shift resulting from the longitudinal shock waves was more likely around the lower values for each motor.

The behavior of the wave strength (Fig. 22), was similar to that of the fraction of dc shift in that it tended to increase with pressure. However, according to the wave strength the star was less stable than the cylinder.

Effect of Grain Configuration (03031-C/-SB/-StC)

The effect of grain configuration on pulse-triggered instability based on the fraction of dc shift and the wave strength for the 03031-C, 03031-SB, and 03031-StC configurations is shown in Figs. 23 and 24.

For pressures below 12.5 MPa the fraction of dc shift and, thus, instability, of the cylinder was the greatest followed by that of the stepped-cylinder and the star (Fig. 23). However, when the stepped-cylinder developed a double-shock system, it had the greatest fraction of dc shift. The concept of double-shock system will be discussed in the Effect of Double Shock section.

In contrast to the fraction of dc shift, the wave strength (Fig. 24) and, thus, instability, of the star was the greatest and that of the stepped-cylinder the smallest. In addition, the wave strength of the stepped-cylinder varied little with pressure. From a designer's perspective, choosing the most stable grain configuration based on this result for wave strength would be extremely misleading given that the time-averaged pressure of the stepped-cylinder became so high that for one motor the casing failed catastrophically.

Effect of Grain Configuration (05057-C/-SB)

The effect of grain configuration on pulse-triggered instability based on the fraction of dc shift and the wave strength for the 05057-C and 05057-SB configurations, is shown in Figs. 25 and 26.

As for the 03031 configurations, the fraction of dc shift (Fig. 25) and, thus, instability of the cylinder was greater than that of the star. However, the difference between the two was less for the 05057 configurations.

The values for wave stength in the case of the star (Fig. 26), spanned those of the cylinder, indicating that they were of similar magnitude.

Effect of Motor Size and Length (Cylinder)

The effect of motor size and length on pulse-triggered instability based on the fraction of dc shift and the wave strength for cylindrical grain configurations is shown in Figs. 27 and 28.

Figure 27 shows that the fraction of dc shift of the smaller diameter motors and, thus, instability, was greater than that of the larger-diameter motor. In addition, the flat profile of the larger-diameter motor differed significantly from that of the smaller ones. Unfortunately, the larger-diameter motor was also longer, introducing an additional variable and resulting in the comparison not being rigorous. From the perspective of the effect of length, the fraction of dc shift of the shorter small-diameter motors and, thus, instability, was greater than that of the longer ones.

As with the fraction of dc shift, the wave strength for the larger-diameter motor (Fig. 28) and, thus, instability, was less than that of the smaller-diameter ones. However, the ranking of the smaller-diameter motors was reversed from the perspective of length with the longer motor having the greater wave strength.

Effect of Motor Size and Length (Star)

The effect of motor size and length on pulse-triggered instability based on the fraction of dc shift and the wave strength for star grain configurations is shown in Figs. 29 and 30.

The fraction of dc shift of the larger-diameter motors (Fig. 29) and, thus, instability, was similar to that of the longer, smaller-diameter star motor. However, the fraction of dc shift of the longer, smaller-diameter motor was less than that of the shorter ones.

On the other hand, the wave strength (Fig. 30) of the larger-diameter motors was less than that of the smaller ones and the longer small-diameter motor had a wave strength greater than the shorter ones.

Effect of Double Shock

The goal of the experimental program was to study single-shock-wave systems. However, a malfunction of the test equipment for motors D7634 and D7607 and the natural tendency of the stepped-cylinder configuration resulted in some double-

Methods for the Solution of Nonlinear Hyperbolic Equations for Resonance Systems," *Journal of Computational Physics*, Vol. 58, No. 1, 1985, pp. 1–28.

[8]Hermsen, R. W., Jamberty, J. T., Jr., and McCormick, R. E., "A Computer Program for the Prediction of Solid Propellant Rocket Motor Performance (SPP) Volume V: User's Manual for the SPP Grain Design and Ballistic Modules." U.S. Air Force Rocket Propulsion Lab., TR-83-036, Sept. 1984.

[9]Harris, P. G., Barrette, S., and Gilbert, N., "Pulse-Triggered Instability in Solid Rocket Motors: Pulser Technology," Defence Research Establishment Valcartier, Rept. 4713/93, Dec. 1993.

[10]Harris, P. G., "Characterization of the Resonant Response of Coated Piezoelectric Pressure Transducers," AIAA Paper 94-3295, June 1994.

[11]Harris, P. G., Hervieux, J. G., Ferland, C., and L'Heureux, C., "Pulse-Triggered Instability in Solid Rocket Motors: Instrumentation and Data Acquisition," Defence Research Establishment Valcartier, Rept. 4650/91, July 1991.